Journal of Power Sources 195 (2010) 5775–5779

Contents lists available at ScienceDirect

Journal of Power Sources

journal homepage: www.elsevier.com/locate/jpowsour

Short communication

Synthesis and performance of $Li_3(V_{1-x}Mg_x)_2(PO_4)_3$ cathode materials

Changsong Dai*, Zhenyu Chen, Haizu Jin, Xinguo Hu

School of Chemical Engineering and Technology, Harbin Institute of Technology, Harbin 150001, PR China

ARTICLE INFO

Article history:
Received 23 September 2009
Received in revised form 22 February 2010
Accepted 26 February 2010
Available online 6 March 2010

Keywords:
Lithium ion battery
Cathode material
Lithium vanadium phosphate
Carbothermal reduction method
Magnesium
Doping

ABSTRACT

In order to search for cathode materials with better performance, $Li_3(V_{1-x}Mg_x)_2(PO_4)_3$ (0, 0.04, 0.07, 0.10 and 0.13) is prepared via a carbothermal reduction (CTR) process with $LiOH{\cdot}H_2O$, V_2O_5, $Mg(CH_3COO)_2{\cdot}4H_2O$, $NH_4H_2PO_4$, and sucrose as raw materials and investigated by X-ray diffraction (XRD), scanning electron microscopic (SEM) and electrochemical impedance spectrum (EIS). XRD shows that $Li_3(V_{1-x}Mg_x)_2(PO_4)_3$ ($x = 0.04$, 0.07, 0.10 and 0.13) has the same monoclinic structure as undoped $Li_3V_2(PO_4)_3$ while the particle size of $Li_3(V_{1-x}Mg_x)_2(PO_4)_3$ is smaller than that of $Li_3V_2(PO_4)_3$ according to SEM images. EIS reveals that the charge transfer resistance of as-prepared materials is reduced and its reversibility is enhanced proved by the cyclic votammograms. The Mg^{2+}-doped $Li_3V_2(PO_4)_3$ has a better high rate discharge performance. At a discharge rate of 20 C, the discharge capacity of $Li_3(V_{0.9}Mg_{0.1})_2(PO_4)_3$ is 107 mAh g^{-1} and the capacity retention is 98% after 80 cycles. $Li_3(V_{0.9}Mg_{0.1})_2(PO_4)_3$//graphite full cells (085580-type) have good discharge performance and the modified cathode material has very good compatibility with graphite.

1. Introduction

Lithium ion batteries have attracted much attention of the electric vehicles R&D departments because they have the highest energy density among all the commercial secondary batteries. For their significant effect on the performance of power lithium ion batteries, cathode materials have become the hotspot of research [1–5]. $LiFePO_4$ has been recognized as the first choice of cathode material for power lithium ion batteries because of its low cost, environmental benignity, cycling stability and high safety [4,5]. However, $LiFePO_4$ has such drawbacks as low discharge voltage (3.5 V), low energy density (380 Wh kg^{-1}), low tap density, poor electronic conductivity and rate capacity, which limit the industrial application of $LiFePO_4$ [6]. In comparison with $LiFePO_4$, monoclinic $Li_3V_2(PO_4)_3$ has better safety performance, higher ionic diffusion coefficient, higher discharge voltage (3.6 V, 4.1 V) and energy density (530 Wh kg^{-1}) [7,8]. Therefore monoclinic $Li_3V_2(PO_4)_3$ is considered as a cathode material better than $LiFePO_4$ and a promising cathode material for power lithium ion batteries used for electric vehicles [8,9]. Monoclinic-phase $Li_3V_2(PO_4)_3$ has $P2_{1/n}$ symmetry and cell parameters $a = 0.8662$ nm, $b = 0.81624$ nm, $c = 1.2104$ nm, and $\beta = 90.452°$ [10]. The structure of $Li_3V_2(PO_4)_3$ is a 3D framework of metal octahedra and phosphate tetrahedra sharing oxygen vertices. Each VO_6 octahedron is surrounded by six PO_4 tetrahedra, whereas each PO_4 tetrahedron is surrounded with four VO_6 octahedra. This configuration forms a 3D network of $(VO_6)_2(PO_4)_3$ units. The Li-ions are located in the cavities within the framework [11].

The structure of monoclinic $Li_3V_2(PO_4)_3$ makes the electronic conductivity and high rate discharge performance poor. Metal ion doping and carbon coating are major methods used to enhance the performance of $Li_3V_2(PO_4)_3$. Metal ion doping (Al^{3+}, Cr^{3+}, Ti^{4+}, Zr^{4+}, Co^{2+} and Fe^{3+}) was investigated through experiment and the doping effects on the reversible capacity and cycle performance of $Li_3V_2(PO_4)_3$ and the doping mechanisms are discussed. Although capacity retention has been improved, the rate capacity still needs to be enhanced [12–17]. Mg doping improves the performance of phosphate materials including $LiFePO_4$ [18] and $LiMnPO_4$ [19], but studies about Mg^{2+} doping effects on $Li_3V_2(PO_4)_3$ have been scarcely carried out. The effect of doping Mg^{2+} in the structure of $Li_3V_2(PO_4)_3$ as well as the performance of the doped $Li_3V_2(PO_4)_3$ cathode materials was investigated in this work.

2. Experimental

2.1. Synthesis and characterization of samples

Samples were prepared using $LiOH{\cdot}H_2O$ (AR, 99%), V_2O_5 (AR, 99%), $Mg(CH_3COO)_2{\cdot}4H_2O$ (AR, 99%), $NH_4H_2PO_4$ (AR, 99%) and a carbon source at a molar ratio of $3.15:(1.00-x):2x:3.00:3.20$. These raw materials were ball milled for 4–7 h with absolute ethyl alcohol. The mixture was then heated to 300 °C with an argon atmosphere

* Corresponding author at: School of Chemical Engineering and Technology, Harbin Institute of Technology, No. 92 West Da-Zhi Street, Harbin 150001, Heilongjiang, PR China. Tel.: +86 451 86413751; fax: +86 451 86413721.
E-mail address: changsd@hit.edu.cn (C. Dai).

0378-7753/$ – see front matter © 2010 Elsevier B.V. All rights reserved.
doi:10.1016/j.jpowsour.2010.02.081

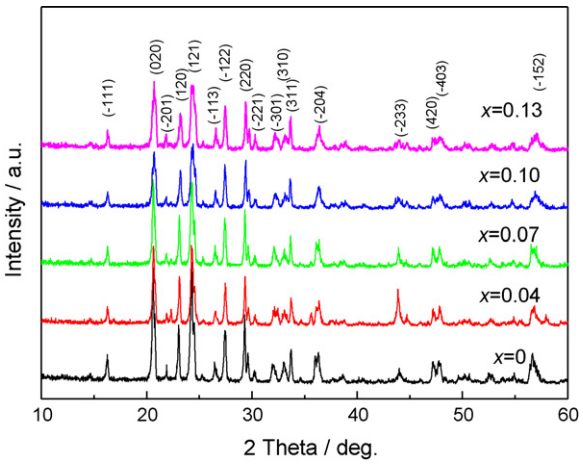

Fig. 1. XRD patterns of $Li_3(V_{1-x}Mg_x)_2(PO_4)_3$ samples.

for 4 h to expel NH_3, H_2O, etc. The mixture was ground after it was cooled down and then heated to and kept at 800 °C with a reducing atmosphere (at an Ar/H_2 volume ratio of 9:1) for 24 h. Then the samples were ground in an agate mortar for later use.

The morphology and particle sizes of the samples were observed with a scanning electron microscope (HITACHI, S-4700). The crystal forms of the samples were confirmed by XRD using a D/max–γ β X' pert diffractometer (Rigaku, Japan) with Cu Kα radiation (λ = 0.154178 nm), a voltage of 45 kV, a current of 50 mA and $2\theta = 10–90°$.

2.2. Assembly of cells and electrochemical measurements

The cathode slurry was prepared by mixing one of the synthesized powders with acetylene black and polyvinylidene fluoride (PVDF) at a mass ratio of 80:10:10 in *n*-methyl-2 pyrrolidone (NMP). Then the cathode slurry was coated on aluminum foil with a thickness of 20 μm. The cathode electrodes were roll-pressed at a pressure of 15 MPa after being dried at 120 °C in vacuum drying for 10–24 h. It was then cut into a wafer (15 mm in diameter). The typical weight of a cathode electrode was 9–10 mg and the cathode electrode is 0.1 mm thick. The anode was lithium metal foil of about 0.30 mm thick. Celgard 2400 with a thickness of about 0.02 mm was used as a separator. $LiPF_6$ of 1 mol L^{-1} in a mixture of EC, DMC and DEC (volume ratio of 1:1:1) was used as the electrolyte. CR2025-type coin cells were assembled in a glove box filled with high-purity argon.

The coin cells were galvanostatically charged and discharged over a voltage range of 3.0–4.3 V at different rates in a multichannel battery test system. The cyclic voltammetry (CV) test was carried out on a CHI-630b electrochemical workstation with a voltage between 3.0 and 4.3 V. The EG&G PARC M 273 and M398 software packages were used in the electrochemical impedance spectroscopy test with a frequency range from 0.1 to 10 kHz. The result was analyzed with the EQUIVCRT software of EG&G. All experiments were carried out at a temperature of 25 ± 0.5 °C.

Table 1
Cell parameters of $Li_3(V_{1-x}Mg_x)_2(PO_4)_3$.

x	*a* (nm)	*b* (nm)	*c* (nm)	*β* (deg.)	Vol. (nm^3)
0	0.86616	0.86068	1.20049	90.3176	0.89494
0.04	0.86106	0.85879	1.21555	90.0035	0.89858
0.07	0.86327	0.85987	1.21106	90.0667	0.89896
0.10	0.85607	0.85655	1.22301	90.2261	0.89679
0.13	0.85517	0.85577	1.23319	90.2454	0.90247

3. Results and discussion

3.1. Characterization of $Li_3(V_{1-x}Mg_x)_2(PO_4)_3$ samples

XRD experiments were conducted to examine the structure changes after $Li_3V_2(PO_4)_3$ was doped with Mg^{2+} to result in $Li_3(V_{1-x}Mg_x)_2(PO_4)_3$ ($x = 0$, 0.04, 0.07, 0.10 and 0.13). As shown in Fig. 1, all the samples had an orderly monoclinic structure, which means that the low dose doping of Mg^{2+} would not alter the structure of materials. Mg^{2+} doping resulted in electron holes in the structure, which would cause *p*-type conductivity [6], and the electronic conductivity of lithium vanadium phosphate was improved. A monotonous dependence of *c* spacing on *x* can be seen from Table 1 that the expansion of *c*-axis may facilitate deintercalation/intercalation of Li^+ ions. As a result, the rate performance of lithium vanadium phosphate was enhanced. Magnesium is electro-

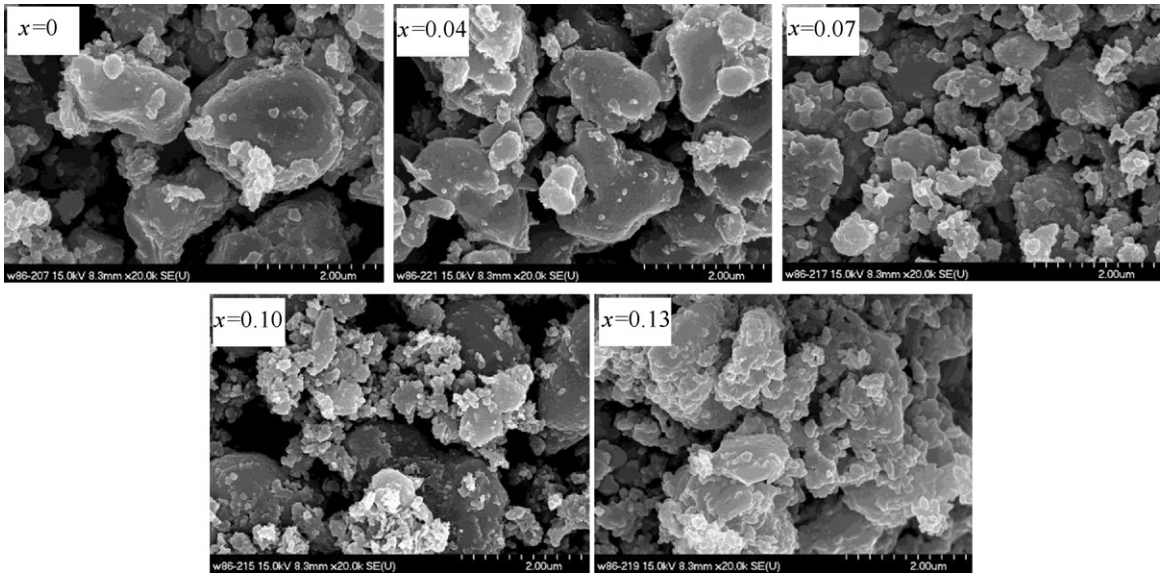

Fig. 2. SEM images of $Li_3(V_{1-x}Mg_x)_2(PO_4)_3$ samples.

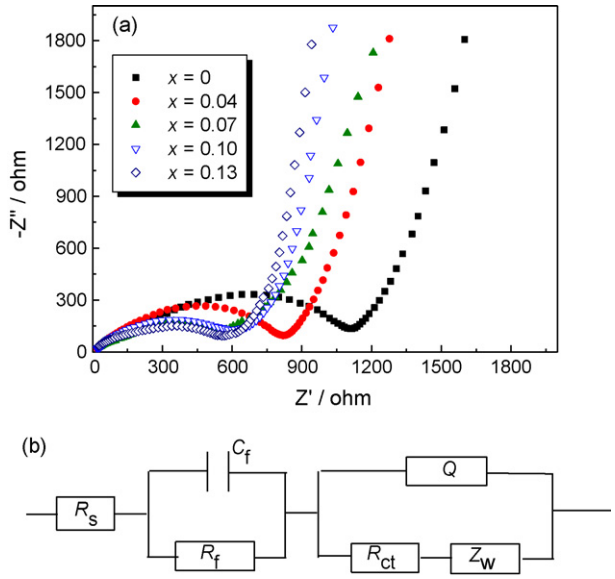

Fig. 3. (a) Nyquist plots of $Li_3(V_{1-x}Mg_x)_2(PO_4)_3$ samples, and (b) equivalent circuit diagram of EIS.

Table 2
Fitting results of EIS.

$Li_3(V_{1-x}Mg_x)_2(PO_4)_3$	$x=0$	$x=0.04$	$x=0.07$	$x=0.1$	$x=0.13$
R_{ct} (Ω)	1226	870	699	650	605

chemically inactive. The substitution of Mg at V site would decrease the initial discharge capacity, and high Mg content may hinder Li^+ diffusion for some Mg^{2+} perhaps occupied the lattice site of Li^+.

As shown in Fig. 2 , the particle of $Li_3(V_{1-x}Mg_x)_2(PO_4)_3$ was smaller than that of $Li_3V_2(PO_4)_3$, and the trend was more obvious with the increase in x. When x was 0.1 or 0.13, the particles agglomerated, it was advantageous to increase the tap density of cathode materials.

3.2. Electrochemical properties of $Li_3(V_{1-x}Mg_x)_2(PO_4)_3$ samples

Electrochemical kinetic property of $Li_3(V_{1-x}Mg_x)_2(PO_4)_3$ was investigated by electrochemical impedance spectroscopy (EIS). As shown in Fig. 3 and Table 2, the charge transfer resistance of $Li_3(V_{1-x}Mg_x)_2(PO_4)_3$ decreased with the increase in x. Exchange current density i^0 is inversely proportional to R_{ct}, and a low R_{ct} means a large i^0. So Mg^{2+} doping could enhance the electrochemical activity of lithium vanadium phosphate. The enhancement was caused by the replacement of V^{3+} by Mg^{2+} in the lattice, which facilitated the electron diffusion.

As shown in Fig. 4, cyclic voltammetry was employed to study the effect of Mg^{2+} doping on the reversibility of $Li_3(V_{1-x}Mg_x)_2(PO_4)_3$. The oxidation peaks of Mg^{2+}-doped $Li_3V_2(PO_4)_3$ moved to the negative direction and the reduction peaks moved to the positive direction. Namely, the potential difference between oxidation peaks and reduction peaks of $Li_3(V_{1-x}Mg_x)_2(PO_4)_3$ was reduced, which indicated the enhancement in reversibility of the electrode reaction by Mg^{2+} doping, and so the insertion and desertion of lithium ions were easier. When $x \geq 0.10$, the two oxidation peaks between 3.5 and 3.7 V (vs. Li^+/Li) and two reduction peaks combined, a result of the decrease in the degree or order of space-occupying by Li^+ and an increase in the insertion–deinsertion activity of lithium ions caused by Mg^{2+} doping.

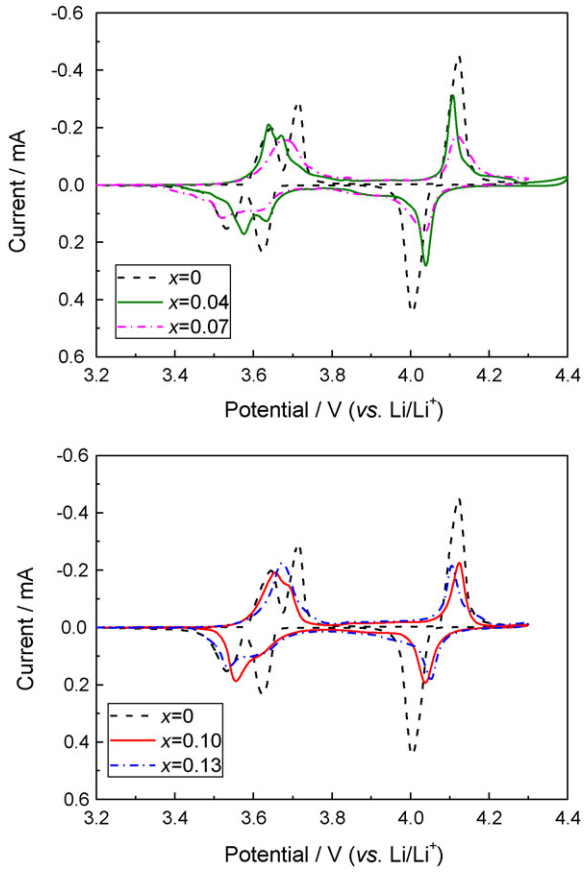

Fig. 4. Cyclic voltammograms of $Li_3(V_{1-x}Mg_x)_2(PO_4)_3$ samples (0.05 mV s^{-1}).

3.3. Electrochemical performance of $Li_3(V_{1-x}Mg_x)_2(PO_4)_3$ samples in half cells

The charge and discharge performances of the $Li_3(V_{1-x}Mg_x)_2(PO_4)_3$ with lithium metal as the anode material were investigated. As shown in Fig. 5, when x was 0.04, the cycle performance of material was not improved while the discharge capacity decreased obviously. The diffusion impedance of $Li_3(V_{0.96}Mg_{0.04})_2(PO_4)_3$ may be large enough to reduce the reversible capacity. The cycle performance of the materials was improved obviously when $x \geq 0.07$. When x was 0.10, the initial discharge specific capacity was 121 mAh g^{-1} maximum and the

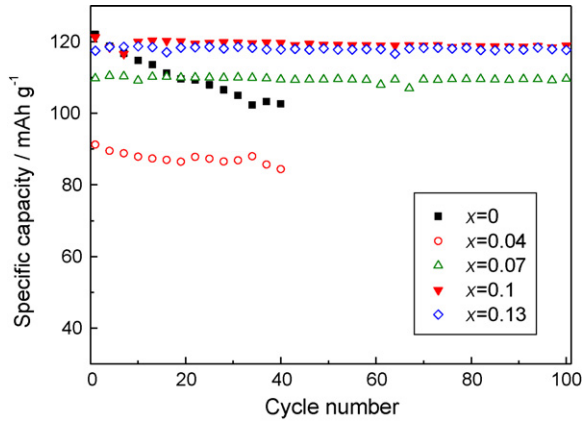

Fig. 5. Cycle performance of $Li_3(V_{1-x}Mg_x)_2(PO_4)_3$ samples at a charge rate and discharge rate of 0.5 C.

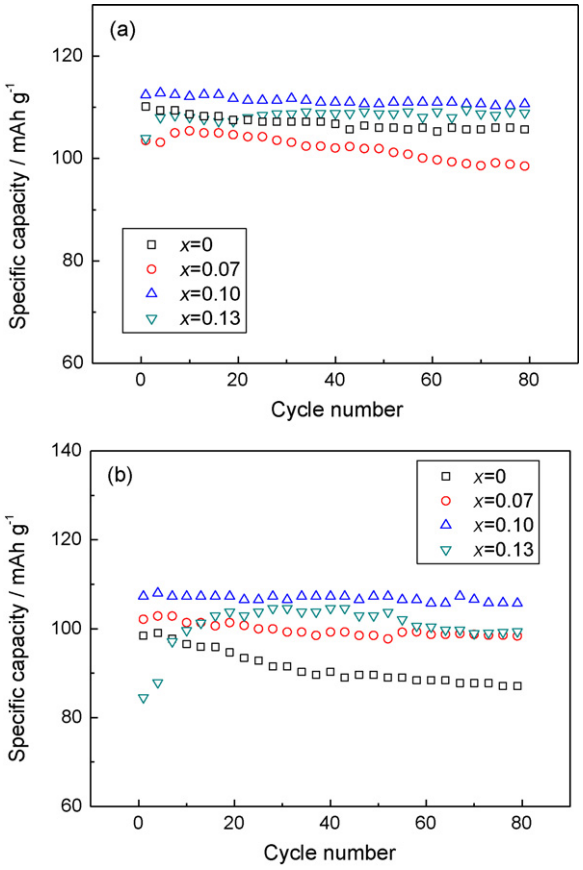

Fig. 6. Cycle performance of $Li_3(V_{1-x}Mg_x)_2(PO_4)_3$ samples (a) at a charge rate of 0.5 C and a discharge rate of 10 C, and (b) at a charge rate of 1 C and a discharge rate of 20 C.

capacity retention was 98% after 100 cycles. When x was 0.13, the cycle performance was still excellent while there was little decrease in the discharge capacity. It can be seen from Fig. 5 that the material showed an excellent cycle performance when x was 0.07, 0.10 or 0.13.

The cycle performance of $Li_3(V_{1-x}Mg_x)_2(PO_4)_3$/Li cell was tested at a high discharge rate to investigate the effect of Mg^{2+} doping. As shown in Fig. 6 these samples showed good high rate discharge performance when x was 0.07, 0.10 or 0.13. As shown in Fig. 6(a), at a charge rate of 0.5 C and a discharge rate of 10 C, the discharge specific capacities in the first cycle of the three samples were 103, 112 and 104 mAh g^{-1}, respectively, and the discharge specific capacities of the three samples were 99, 111 and 109 mAh g^{-1}, respectively, after 80 cycles. As shown in Fig. 6(b), at a charge rate of 1 C and a discharge rate of 20 C, the discharge specific capacities in the first cycle of the three samples were 102, 107 and 85 mAh g^{-1}, respectively, and the discharge specific capacities of the three samples were 98, 106 and 99 mAh g^{-1}, respectively, after 80 cycles. These samples showed excellent cycle performance. When x was 0.10, there was a significant improvement in the rate capacity and cycle performance of Mg^{2+}-doped lithium vanadium phosphate at a high discharge rate.

$Li_3(V_{0.9}Mg_{0.1})_2(PO_4)_3$ had an excellent high rate discharge performance, but its high rate charge performance was not fully studied yet. Cyclic voltammetry was employed at a scan rate of 0.36 mV s^{-1} to investigate the electrochemical behavior of $Li_3(V_{0.9}Mg_{0.1})_2(PO_4)_3$ and $Li_3V_2(PO_4)_3$ at high charge and discharge rates. As shown in Fig. 7, at a high scan rate, reversibility was enhanced by Mg^{2+} doping and the two oxidation peaks between 3.5 and 3.9 V (vs. Li^+/Li) combined. A charge–discharge test was carried

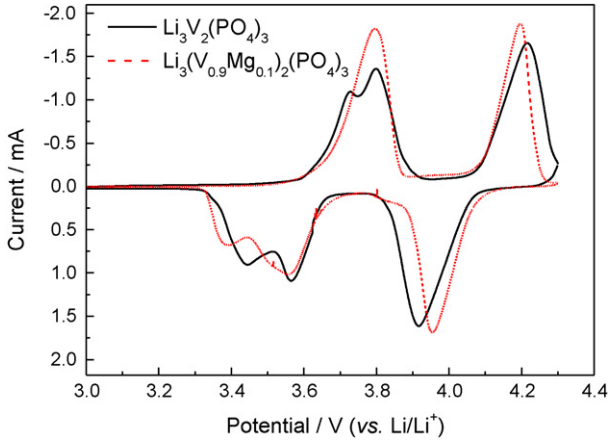

Fig. 7. Cyclic voltammograms of $Li_3(V_{0.9}Mg_{0.1})_2(PO_4)_3$ and $Li_3V_2(PO_4)_3$ samples (0.36 mV s^{-1}).

out to confirm this result. As shown in Fig. 8(a), at a charge rate of 4 C and the discharge rate of 5 C, the initial discharge specific capacity was 114 mAh g^{-1}, when the charge and discharge rates were both 10 C, the initial discharge specific capacity was 98 mAh g^{-1}. Fig. 8(b) shows the cycle performance of the $Li_3(V_{0.9}Mg_{0.1})_2(PO_4)_3$/Li cell at a charge rate of 4 C and a discharge rate of 5 C, and both a charge and a discharge rate of 10 C. It can be seen in Fig. 8 that $Li_3(V_{0.9}Mg_{0.1})_2(PO_4)_3$ shows good electrochemical performance in both high rate discharge and high rate charge.

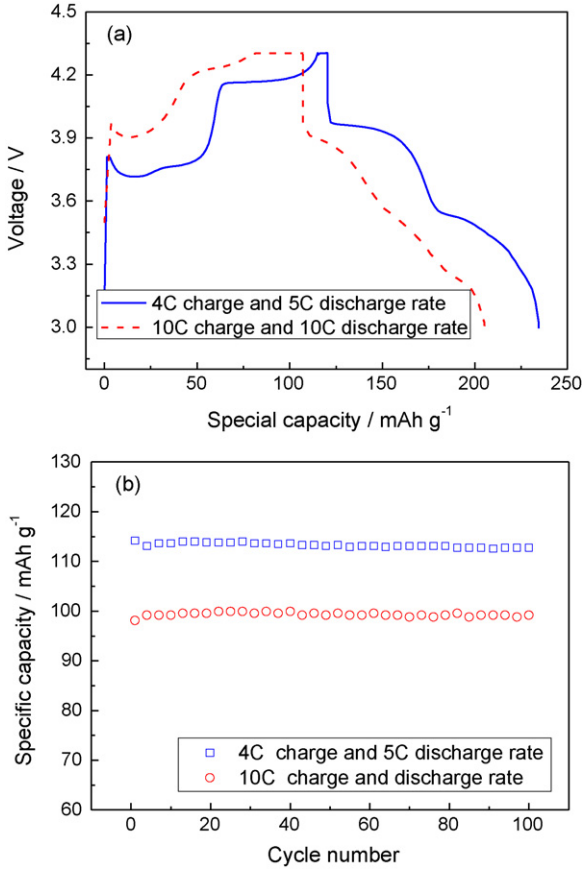

Fig. 8. (a) Initial charge–discharge curves and (b) cycle performance of $Li_3(V_{0.9}Mg_{0.1})_2(PO_4)_3$ samples at a charge rate of 4 C and a discharge rate of 5 C and at a charge rate and a discharge rate of 10 C.

Table 3
Parameters and test results of $Li_3(V_{0.9}Mg_{0.1})_2(PO_4)_3$//graphite full cells (085580-type, at 1 C rate).

Item	Performance
Size (thickness × width × height)	8 mm × 55 mm × 80 mm
Capacity of the cell	1930 mAh
Internal resistance	9 mΩ
Volumetric specific energy	182 Wh L^{-1}
Mass specific energy	96 Wh kg^{-1}

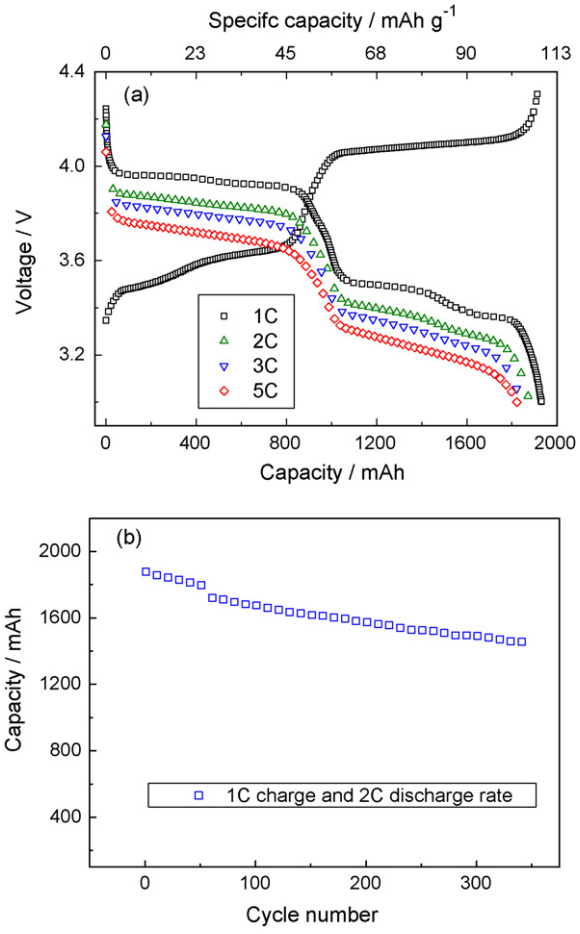

Fig. 9. (a) High rate discharge performance, and (b) cycle performance of $Li_3(V_{0.9}Mg_{0.1})_2(PO_4)_3$ samples in full cells.

3.4. Electrochemical performance of $Li_3(V_{0.9}Mg_{0.1})_2(PO_4)_3$ sample in full cells

The electrochemical performance in full cells was investigated with $Li_3(V_{0.9}Mg_{0.1})_2(PO_4)_3$//graphite cells (085580-type), and the basic information of the cells is listed in Table 3. As shown in Fig. 9(a) at a charge rate of 1 C and discharge rates of 1, 2, 3, and 5 C, the discharge specific capacities in the first cycle of the cells were 109, 106, 104 and 103 mAh g^{-1}, respectively. It can be seen from Fig. 9(b) that at a charge rate of 1 C and a discharge rate of 2 C, the discharge specific capacity in the first cycle was 106 mAh g^{-1}, and the discharge specific capacity was 82 mAh g^{-1} after 345 cycles. It can be seen from Fig. 9 that $Li_3(V_{0.9}Mg_{0.1})_2(PO_4)_3$//graphite cells show not only excellent high rate discharge performance, but also good cycle performance.

4. Conclusions

$Li_3(V_{1-x}Mg_x)_2(PO_4)_3$ (x = 0.04, 0.07, 0.10 and 0.13), which was synthesized by a CTR method, has the same monoclinic structure as the undoped $Li_3V_2(PO_4)_3$ and the expansion of c-axis can be seen with the dose of Mg^{2+} increased. After Mg^{2+} doping the samples had a smaller particle size, a lower charge transfer resistance and enhanced reversibility. The as-prepared $Li_3(V_{1-x}Mg_x)_2(PO_4)_3$ exhibited excellent high rate discharge performance. At a discharge rate of 20 C, the discharge specific capacity of $Li_3(V_{0.9}Mg_{0.1})_2(PO_4)_3$ was 107 mAh g^{-1} and the capacity retention was 98% after 80 cycles. The investigation of $Li_3(V_{0.9}Mg_{0.1})_2(PO_4)_3$//graphite full cells demonstrated a good discharge performance and the modified cathode material had very good compatibility with graphite.

References

[1] T. Ohzuku, A. Ueda, J. Electrochem. Soc. 141 (1994) 2972–2977.
[2] T. Nohma, H. Kurokawa, M. Uehara, M. Takahashi, K. Nishio, T. Saito, J. Power Sources 54 (1996) 522–524.
[3] T. Ohzuku, S. Kitano, M. Iwanaga, H. Matsuno, A. Ueda, J. Power Sources 68 (1997) 646–651.
[4] A.K. Padhi, K.S. Nanjundaswamy, J.B. Goodenough, J. Electrochem. Soc. 144 (1997) 1188–1194.
[5] J.M. Tarascon, M. Armand, Nature 414 (2001) 359–367.
[6] S.Y. Chung, J.T. Bloking, Y.M. Chiang, Nat. Mater. 1 (2002) 123–128.
[7] H. Huang, S. Yin, T. Kerr, N. Taylor, L.F. Nazar, Adv. Mater. 14 (2002) 1525–1528.
[8] H. Huang, T. Faulkner, J. Barker, M.Y. Saidi, J. Power Sources 189 (2009) 748–751.
[9] L. Wang, L.C. Zhang, I. Lieberwirth, H.W. Xu, C.H. Chen, Electrochem. Commun. (2009), doi:10.1016/j.elecom.2009.10.034.
[10] L.S. Cahill, R.P. Chapman, J.F. Britten, G.R. Goward, J. Phys. Chem. B 10 (2006) 7171–7177.
[11] M.Y. Saidi, J. Barker, H. Huang, J.L. Swoyer, G. Adamson, J. Power Sources 119–121 (2003) 266–272.
[12] D. Morgan, G. Ceder, M.Y. Saidi, J. Barker, J. Swoyer, H. Huang, G. Adamson, J. Power Sources 119–121 (2003) 755–759.
[13] Y.H. Chen, Y.M. Zhao, X.N. An, J.M. Liu, Y.Z. Dong, L. Chen, Electrochim. Acta 54 (2009) 5844–5850.
[14] S.Q. Liu, S.C. Li, K.L. Huang, Z.H. Chen, Acta Phys. Chim. Sin. 23 (2007) 537–542.
[15] M. Sato, H. Ohkawa, K. Yoshida, M. Saito, K. Uematsu, K. Toda, Solid State Ionics 135 (2000) 137–142.
[16] Q. Kuang, Y.M. Zhao, X.N. An, J.M. Liu, Y.Z. Dong, L. Chen, Electrochim. Acta (2009), doi:10.1016/j.electacta.2009.10.028.
[17] M.M. Ren, Z. Zhou, Y.Z. Li, X.P. Gao, J. Yan, J. Power Sources 162 (2006) 1357–1362.
[18] M.R. Yang, W.H. Ke, J. Electrochem Soc. 155 (2008) A729–A732.
[19] T. Shiratsuchi, S. Okada, T. Doi, J.I. Yamaki, Electrochim. Acta 54 (2009) 3145–3151.